Landau-Zener-Stückelberg Interferometry in Quantum Dots with Fast Rise Times: Evidence for Coherent Phonon Driving

M. Korkusinski, S. A. Studenikin, G. Aers, G. Granger, A. Kam, and A. S. Sachrajda
Security and Disruptive Technologies, National Research Council Canada, Ottawa, K1A 0R6, Canada
(Received 25 August 2016; published 8 February 2017)

Manipulating qubits via electrical pulses in a piezoelectric material such as GaAs can be expected to generate incidental acoustic phonons. In this Letter we determine theoretically and experimentally the consequences of these phonons for semiconductor spin qubits using Landau-Zener-Stückelberg interferometry. Theoretical calculations predict that phonons in the presence of the spin-orbit interaction produce both phonon-Rabi fringes and accelerated evolution at the singlet-triplet anticrossing. Observed features confirm the influence of these mechanisms. Additionally, evidence is found that the pulsed gates themselves act as phonon cavities increasing the influence of phonons under specific resonant conditions.

DOI: 10.1103/PhysRevLett.118.067701

Gated quantum dot devices are promising candidates for quantum information processing. Encoding the information can provide individual qubit addressability, all-electrical operation, and robustness against decoherence related to the hyperfine interaction or random charge instabilities [1,2]. Coherent control of such coded qubits has recently been demonstrated in double-dot [2–6] and triple-dot systems [7–10].

In the piezoelectric GaAs/AlGaAs system, charge fluctuations may be expected to lead to phonon generation. Phonons believed to originate from inherent charge fluctuations in nearby quantum point contacts were recently shown to interact coherently with confined electrons in double and triple quantum dot devices [11–13]. In this Letter we study the influence on the qubit state dynamics of phonons generated by the very pulses used to manipulate the qubits. We focus on the two-electron singlet-polarized triplet (S/T_+) system and probe it with Landau-Zener-Stückelberg (LZS) interferometry [4,7]. The two states are coupled by hyperfine interaction with nuclear spins. We drive the S/T_+ system through the resulting anticrossing with a detuning pulse with a very short rise time, for which the LZS interference pattern is not expected. This pulse is translated into a nontrivial population of high-energy acoustic phonons as a result of the piezoelectric effect. These phonons provide a resonant coupling mechanism between S and T_+ via the electron-phonon and spin-orbit interactions. We expect that the resulting S/T_+ dynamics will be modified from its usual LZS pattern by effects depending on the occupations of the phonon modes. Here we show that the phonon coupling (i) accelerates the dynamics of the S/T_+ system close to the hyperfine anticrossing, manifesting as an apparent increase of the gap, (ii) creates new LZS interference fringes away from the anticrossing, and (iii) in case of cavity phonon modes, leads to the appearance of discrete resonances when the S/T_+ energy separation equals the energy of the cavity phonon.

Figure 1(a) shows the gate layout of our lateral triple dot device. Details of previous LZS experiments with our sample are given elsewhere [7,8]. The gates are tuned to a double dot regime in which two electronic configurations, with electron numbers $(N_L, N_C, N_R) = (1,1,1)$ and (2,0,1), are close in energy and an electron in one of the dots (white circle) acts as a spectator. We classify the energy levels by the total spin of the two "active" electrons as S (singlet) and T_+ (polarized triplet). The system is pulsed by applying detuning voltages dV_1 and dV_2, opposite in sign, to gates 1 and 2, respectively. Figure 1(b) plots the experimentally calibrated energy diagram of the system as a function of detuning $\Delta V(dV_1, dV_2)$ [7,8]. A magnetic field $B = 200$ mT was used. Ignoring the trapped electron in the right-hand dot,

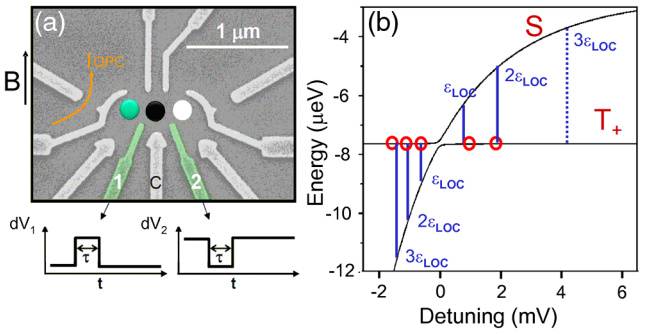

FIG. 1. (a) Scanning electron micrograph of the gates composing the triple-dot gated lateral device. The sample is maintained at the temperature of ~80 mK. The S/T_+ system is set up with the left-hand and middle dots, while the right-hand dot is inert in the relevant range of detunings. The detuning pulse is applied to the gates 1 and 2. (b) Energy of the singlet S and polarized triplet T_+ as a function of the detuning between the left-hand and center dots. Blue lines indicate detunings corresponding to absorption of phonons with energy being a multiple of 1.3 μeV. Red circles show the energies extracted from Fig. 4 (a) (see text for discussion).

the triplet state $T_+(1,1)$ is a configuration containing one electron per dot, with both electrons in a spin up state. Its energy, E_T, is the reference level in Fig. 1(b). The singlet state is a linear combination of two configurations: $S(2,0)$, with two electrons in the left dot with antiparallel spins, and $S(1,1)$ with one electron per dot. Because of interdot tunneling, the singlet energy E_S can be tuned with respect to E_T by gate voltages dV_1, dV_2, as evident in Fig. 1(b).

Following Taylor *et al.* [2], we describe our two-level system with the effective Hamiltonian

$$\hat{H}_0 = \begin{bmatrix} E_S & \Delta B_X \\ \Delta B_X & E_T \end{bmatrix}. \quad (1)$$

Here, $\Delta B_X \approx 0.1$ μeV is the effective singlet-triplet coupling due to hyperfine interaction with the nuclear spins of underlying material. This coupling leads to the small anticrossing of S and T_+ levels visible in Fig. 1(b). The derivation of Eq. (1) is given in Ref. [14].

In the LZS interferometry experiment [7] the system is prepared in the S state in the regime where $E_S < E_T$. Next, the detuning pulse of duration τ is applied, casting the system in a time-dependent state $|\Psi(t)\rangle = \alpha_{20}(t)|S(2,0)\rangle + \alpha_{11}(t)|S(1,1)\rangle + \beta(t)|T_+(1,1)\rangle$. The accumulation of amplitudes and phases is analyzed via spin-to-charge conversion by measuring $|\alpha_{2,0}|^2$ after the pulse by the charge detection technique [18]. The amount of mixing due to hyperfine coupling depends on the pulse rise time τ_s, which must be comparable to $\sim\hbar/2\Delta B_X$ for LZS interference to be observable. A faster pulse nonadiabatically drives the system through the anticrossing resulting in $\beta(t) \approx 0$ throughout.

The phonon-mediated S/T_+ coupling is due to the spin-orbit (SO) interaction, connecting the $S(2,0)$ and $T_+(1,1)$ configurations. The SO Rashba [19] and Dresselhaus [20] couplings are characterized respectively by the Hamiltonians [21] $\hat{H}_R = \alpha_{\rm SO}(\hat{\sigma_x}\hat{p}_y - \hat{\sigma}_y\hat{p}_x)$ and $\hat{H}_D = \beta_{\rm SO}(\hat{\sigma_y}\hat{p}_y - \hat{\sigma}_x\hat{p}_x)$, with $\alpha_{\rm SO}$ and $\beta_{\rm SO}$ being material parameters, and $\hat{p}_i$, $\hat{\sigma}_i$ being the ith component of the momentum and spin operators, respectively. Here, the spin flip occurs as the electron tunnels between dots. SO interactions enhance the S/T_+ hyperfine gap by renormalizing the term ΔB_X in Eq. (1) [14]. The interplay of the two couplings in S/T_+ dynamics has been examined experimentally [5].

Electron tunneling is enabled by the bath of acoustic phonons. We account for it by introducing two additional Hamiltonian components $\hat{H}_{\rm ph} + \hat{H}_{e-{\rm ph}} = \sum_{\vec{q}} \varepsilon(q)\hat{b}^+_{\vec{q}}\hat{b}_{\vec{q}} + \sum_{\vec{q}}\sum_{ij\sigma} M_{ij}(\vec{q})(\hat{b}_{\vec{q}} + \hat{b}^+_{-\vec{q}})\hat{c}^+_{i\sigma}\hat{c}_{j\sigma}$. The first term introduces the energies of quantized phonons, and we take the phonon energy $\varepsilon(\vec{q}) = \hbar v_s|\vec{q}|$, where v_s is the two-dimensional speed of sound at the sample heterointerface, and $\hat{b}^+_{\vec{q}}$ ($\hat{b}_{\vec{q}}$) is the creation (annihilation) of the two-dimensional phonon with wave vector $\vec{q}$. The second term describes electron-phonon coupling, involving electron scattering (without spin flip) accompanied by absorption or emission of a phonon, with $\hat{c}^+_{i\sigma}$ ($\hat{c}_{i\sigma}$) being the creation (annihilation) operator of an electron in dot i with spin σ. This Hamiltonian is scaled by the matrix element $M_{ij}(\vec{q})$ (Refs. [21,22]), whose form (piezoelectric or deformation) is discussed elsewhere [14]. Here we emphasize the existence of the element $M_{\rm LR}(\vec{q})$ enabling the phonon-assisted tunneling between dots.

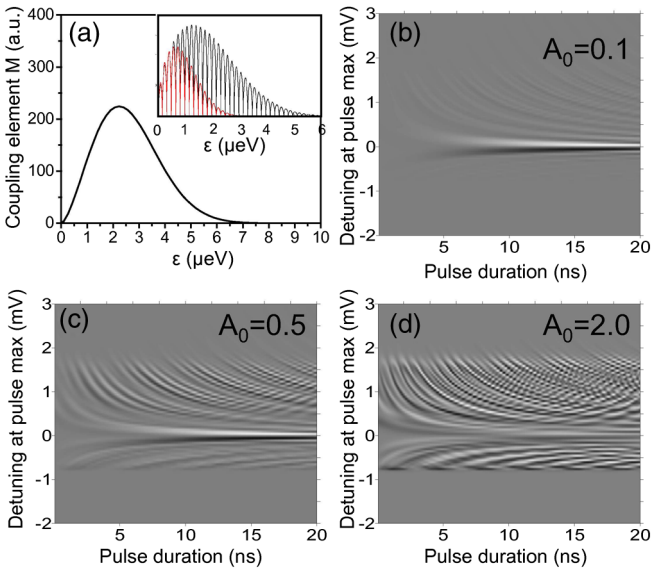

FIG. 2. LZS interference calculated for the S/T_+ system in the bath of phonons. (a) Model electron-phonon coupling element M reflecting the phonon mode population at pulse rise time $\tau_s = 1$ ns. Inset: Phonon energy resolved strength of electron-phonon coupling via the deformation potential computed using the Fourier transform of the pulse with duration $\tau = 25$ ns for rise times 1 ns (black) and 2 ns (red). Grayscale plots of derivative dP/dV_1 of the probability of finding the system in the singlet state as a function of detuning at pulse maximum (relative to S/T_+ anticrossing) and pulse duration for phonon strength factor $A_0 = 0.1$ (b), 0.5 (c), and 2 (d). The pulse rise time $\tau_s = 1$ ns.

The phonon population $n(\varepsilon)$ due to the pulse is estimated phenomenologically as proportional to the Fourier transform of the pulse. The inset in Fig. 2(a) shows this transform for pulse rise times $\tau_s = 1$ ns (black) and 2 ns (red), as a function of energy scaled by the deformation-type phonon coupling. The realistic Gaussian profile of pulse edges was taken [23]. Shorter pulse rise times result in a higher average phonon energy and an increase of the population of higher-energy modes. The fast oscillations are due to the pulse length ($\tau = 25$ ns was used). Evidently, the pulse results in a nontrivial phonon population over a large energy range, which prohibits us from treating phonons as quantized particles. Instead, in the Hamiltonian $\hat{H}_0$ we replace the static term ΔB_X by a time-dependent coupling $\Delta B_X + \sum_\omega \hbar\omega n(\omega)A(\omega)\sin(\omega t)$. We decompose $n(\omega)A(\omega) = A_0 M(\omega)\zeta(\omega)$, where A_0 is a phenomenological phonon strength parameter, $M(\omega)$ is the phonon

population multiplied by energy-dependent material parameters (related to the electron-phonon coupling element M_{LR} discussed earlier), and $\zeta(\omega)$ is the SO-related spectral factor describing the relative content of singly- and doubly-occupied configurations in the electronic states [14]. Figure 2(a) shows the energy dependence of the factor $M(\omega)$ for the pulse rise time $\tau_s = 1$ ns.

Now we demonstrate that the presence of phonons accelerates the S/T_+ dynamics at the hyperfine anticrossing. We prepare our system with $E_S = E_T$ (no pulse) and derive the singlet probability of the driven Rabi system as $|\langle S|\Psi(t)\rangle|^2 = \cos^2[\Delta B_X t/\hbar + \sum_\omega n(\omega)A(\omega)(1-\cos(\omega t))]$, assuming an initial state $|S\rangle$. In the absence of phonons this evolution reduces to the free Rabi flopping in the hyperfine field at the anticrossing. The presence of phonons modifies this time evolution increasingly as the phonon population $n(\omega)$ increases. In particular, we find that as the LZS pulse drives the system through the anticrossing region, its state evolves into an S/T_+ superposition faster than it would in the hyperfine field alone. Thus, in the presence of the phonon bath the system behaves as if the effective gap accompanying the S/T_+ anticrossing were increased. To demonstrate this, we have solved numerically the time-dependent problem [7] $d\hat{\varrho}(t)/dt = i[\hat{\varrho}(t), \hat{H}/\hbar]$ with the density matrix $\hat{\varrho}(t)$ and the effective Hamiltonian accounting for the pulse. We choose the pulse rise time $\tau_s = 1$ ns, and only take into account the phonon mode with energy equal to the S/T_+ gap corresponding to the detuning when the pulse is at its peak. In Fig. 2 we show the singlet probability amplitude as a function of detuning at pulse maximum (vertical axis, relative to the position of S/T_+ anticrossing) and pulse duration τ (horizontal axis) for $A_0 = 0.1$ [(b), almost no phonons], $A_0 = 0.5$ (c), and $A_0 = 2$ (d). We see a near absence of the LZS pattern in the first case, while the increase of phonon population leads to a strong reappearance of the LZS pattern.

In the left-hand panels of Fig. 3 we plot experimental LZS interference traces for different pulse rise times as a function of detuning at maximum and duration τ of the pulse. With a constant S/T_+ anticrossing gap and no phonon effects, we would expect the LZS oscillations to disappear as τ_s is decreased. We observe dramatically more complex behavior. To reproduce the experimental observation of LZS spectra in numerical simulations without adding SO or electron-phonon coupling, it is necessary to increase artificially the anticrossing gap Δ as τ_s is decreased. The results of these simulations are shown in the right-hand panels of Fig. 3. While for long pulse rise times [Figs. 3(a) and 3(b)], the effective gap is equal to the hyperfine gap, $\Delta = 2\Delta B_X = 0.2$ μeV, for the shortest rise time, $\tau_s = 0.2$ ns, this apparent gap needs to be increased to $\Delta = 0.66$ μeV. This demonstrates the speeding up of the coherent S/T_+ dynamics by phonon modes and the corresponding persistence of the LZS oscillations. We note that in Fig. 3 the position of the anticrossing does not change, which confirms that dynamic nuclear polarization does not play any role in these new phenomena.

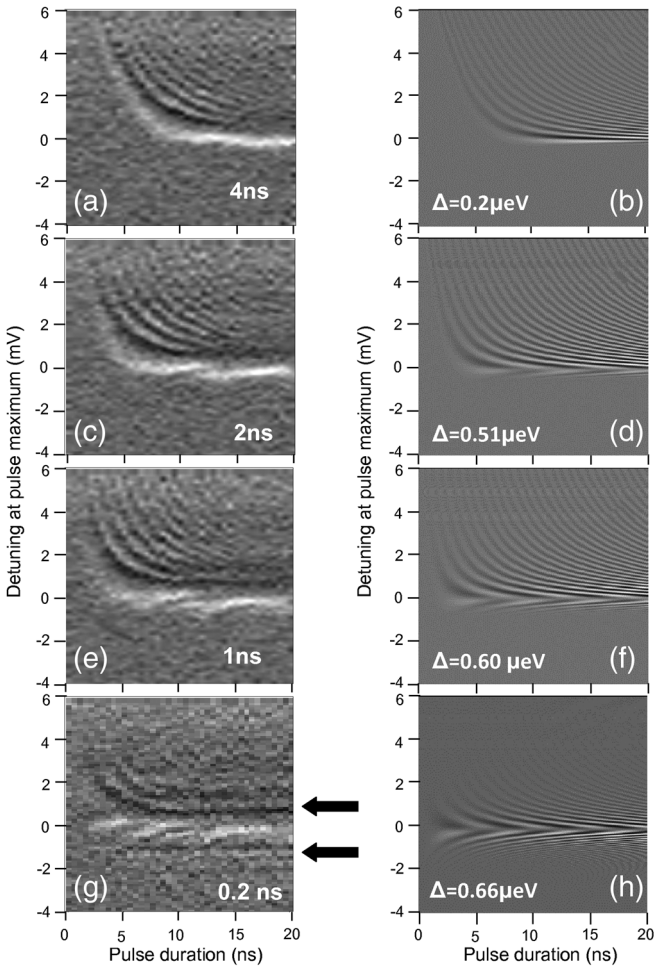

FIG. 3. LZS oscillations revealed by the singlet amplitude observed in experiment (left-hand panels) and calculated (right-hand panels) as a function of the duration and detuning at maximum of the pulse for the pulse rise times $\tau_s = 4$ ns (a),(b), 2 ns (c),(d), 1 ns (e),(f), and 0.2 ns (g),(h). The time delay between consecutive pulses was $T_m = 2$ μs. The calculations did not include phonon effects, but were performed with a varying hyperfine gap Δ. Black arrows mark the horizontal resonances due to discrete phonon modes.

Now we focus on the region of negative detunings (lower part of the LZS graphs). Here, the simulations not including phonons, shown in Fig. 3, predict weak interference fringes, while both experiment and time-dependent simulations including SO-phonon effects shown in Fig. 2 reveal strong features, which differ from the regular LZS oscillations. The new features are white traces in the experimental diagrams of Fig. 3 and are emphasized by red dashed lines in Fig. 4(a). Specifically, in Fig. 3, for $\tau_s = 4$ ns we see only LZS oscillations, while for $\tau_s = 2$ ns the lowest edge of the pattern breaks into two stripes, for $\tau_s = 1$ ns—into three, and for $\tau_s = 0.2$ ns there are four stripes. In Fig. 4(a) the stripes are even more numerous. The new fringes can be understood from the effective Hamiltonian taken at $E_S \ll E_T$. The states

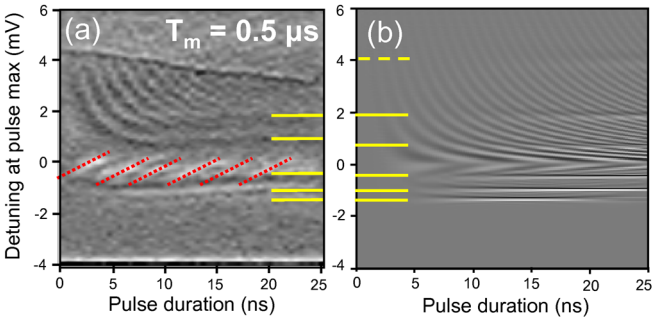

FIG. 4. (a) LZS oscillations measured with the rise time $\tau_s = 1$ ns and the time between pulses $T_m = 0.5$ μs. Red dashed lines: interference pattern resulting from driving by the phonon bath away from S/T_+ crossing. Yellow lines: fringes due to the discrete phonon modes. The strong line in the top part is an experimental artifact. (b) LZS oscillations calculated with localized phonon modes, but no phonon bath.

$|S\rangle$ and $|T_+\rangle$ are then mixed only by the SO-phonon mechanism, and we have the Rabi problem, exhibiting a Lorentzian resonance for phonon energy $\hbar\omega_q = |E_S - E_T|$. At this energy, the singlet probability is $|\langle S|\Psi(t)\rangle|^2 = \cos^2[\omega_q n(\omega_q)A(\omega_q)t]$ for a system at $t = 0$ in the state $|S\rangle$. This interference process, driven by the phonon population and electron-phonon coupling, is absent in the conventional LZS experiment. Since the phonon bath has continuous distribution of mode energies, for any relevant pulse amplitude there will exist a resonant phonon mode and the system will experience resonant Rabi driving. Note the corresponding new fringes for positive detunings are obscured by regular LZS oscillations leading to the asymmetric appearance of features around zero detuning. As described above, LZS oscillations are observed at short pulse rise times due to the influence of the phonons on the dynamics of the system at the anticrossing.

The third signature of phonons is seen experimentally as horizontal fringes, denoted by black arrows in Fig. 3(g), and yellow stripes in Fig. 4(a). In Fig. 1(b) we mark their positions as red circles on the experimentally calibrated S/T_+ energy diagram. They correspond well to an equally spaced ladder of energies on either side of the anticrossing, with spacing $\varepsilon_{\mathrm{LOC}} = 1.3$ μeV (the vertical blue lines). With phonon velocity $v_s = 2.7 \times 10^9$ μm/s, these energies correspond to phonon half-wavelengths being integer fractions of $L_{\mathrm{LOC}} = 4.3$ μm. In our sample layout in Fig. 1(a) we find the narrow components of the pulsed gates marked in green are approximately of length L_{LOC} [14]. Thus, these gates appear to act as phonon cavities producing discrete phonon modes which couple to our electronic system. For detunings for which the singlet-triplet energy gap is a multiple of $\varepsilon_{\mathrm{LOC}}$, the LZS interferometry produces a phonon-assisted singlet-triplet resonance. To model these resonant features, we assume a localized phonon mode with the momentum $\vec{Q}$, energy $\varepsilon(\vec{Q})$, and occupation $n(\vec{Q})$. We use the Hamiltonian $\hat{H} = \hat{H}_0 + \hat{H}_{\mathrm{SO}} + \hat{H}_{\mathrm{ph}} + \hat{H}_{e-\mathrm{ph}}$ in the quantized phonon picture. Through the second-order SO-phonon process, this mode creates a resonance when the energy of the state $|S\rangle|n(\vec{Q})\rangle$ is equal to that of $|T_+\rangle|n(\vec{Q}) - 1\rangle$ or $|T_+\rangle|n(\vec{Q}) + 1\rangle$, depending on the ordering of energies. We expect a signature of this incoherent phonon absorption or emission process appearing at the detuning for which $|E_S - E_T| = \varepsilon(\vec{Q})$ irrespectively of the duration of the pulse, so long as the mode $\vec{Q}$ is populated. To confirm this, we performed numerical simulations of the LZS interference in the presence of localized phonon modes, but omitting the phonon bath. The result is shown in Fig. 4(b). We recover the horizontal features at detunings corresponding to experiment although the weak $3\varepsilon_{\mathrm{LOC}}$ peak indicated by the dashed yellow line is not observed.

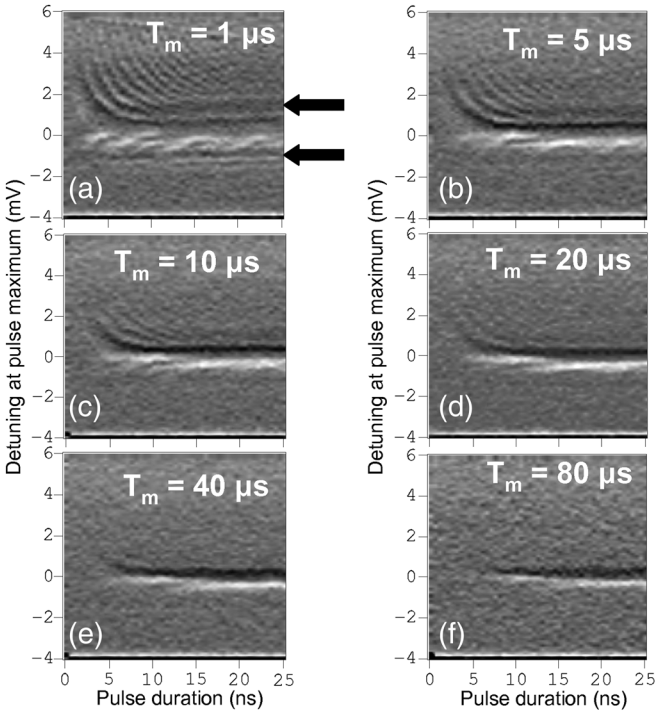

FIG. 5. LZS oscillations measured with a constant pulse rise time $\tau_s = 1$ ns, as a function of the delay between pulses T_m, for $T_m = 1$ μs (a), 5 μs (b), 10 μs (c), 20 μs (d), 40 μs (e), and 80 μs (f). The line appearing near the top of panel (a) is an experimental artifact.

To demonstrate experimentally that all the new features are indeed related to phonons generated by the pulse, we measure LZS oscillations with a constant rise time $\tau_s = 1$ ns, but vary the time delay T_m between consecutive pulses allowing phonon diffusion and dissipation to suppress the buildup of the phonon population. Figure 5 shows the resulting LZS diagrams. For short times T_m we observe the complex pattern discussed previously. As T_m becomes longer, the phonons have enough time to dissipate, leading to the gradual disappearance of the LZS pattern. For the longest time T_m we recover the result expected in the

absence of phonons for this rise time. The long dwell time near the S/T_+ system (tens of μs) suggests that the phonons undergo multiple reflections from the edges of the sample (~3 mm away from the confined electrons) before their energy dissipates [24].

In conclusion, we have demonstrated theoretically and experimentally the consequences of phonons generated by the very pulses used to manipulate spin qubits in gated AlGaAs/GaAs quantum dots in combination with the spin-orbit interaction. Our results indicate that under these commonly achieved experimental conditions we observe coherent hybrid interplay between phonon and spin quantum platforms. Existence of spin-nonflipping SO terms [25] is expected to enable a similar mechanism in S/T_0 two-electron, and (2,1) charge-spin hybrid systems [26]. In (1,1,1) exchange-only qubits, both logical qubit states have the same total spin [8,27], opening the possibility of dynamical driving by phonons alone. These effects need to be taken into account in the design of quantum circuits and interpretation of results, and may lead to new experimental manipulation possibilities. Incoherent effects related to phonon cavity modes were also observed and discussed.

We acknowledge useful discussions with G. Platero, H. Ribeiro, and W. Coish. We thank Z. Wasilewski for the sample wafer and P. Zawadzki for technical assistance with cryogenics.

[1] D. Bacon, J. Kempe, D. A. Lidar, and K. B. Whaley, Phys. Rev. Lett. **85**, 1758 (2000).
[2] J. M. Taylor, J. R. Petta, A. C. Johnson, A. Yacoby, C. M. Marcus, and M. D. Lukin, Phys. Rev. B **76**, 035315 (2007).
[3] J. R. Petta *et al.*, Science **309**, 2180 (2005).
[4] J. R. Petta, H. Lu, and A. C. Gossard, Science **327**, 669 (2010).
[5] J. M. Nichol, S. P. Harvey, M. D. Shulman, A. Pal, V. Umansky, E. I. Rashba, B. I. Halperin, and A. Yacoby, Nat. Commun. **6**, 7682 (2015).
[6] K. Ono, D. G. Austing, Y. Tokura, and S. Tarucha, Science **297**, 1313 (2002).
[7] S. A. Studenikin, G. C. Aers, G. Granger, L. Gaudreau, A. Kam, P. Zawadzki, Z. R. Wasilewski, and A. S. Sachrajda, Phys. Rev. Lett. **108**, 226802 (2012).
[8] L. Gaudreau, G. Granger, A. Kam, G. C. Aers, S. A. Studenikin, P. Zawadzki, M. Pioro-Ladrière, Z. R. Wasilewski, and A. S. Sachrajda, Nat. Phys. **8**, 54 (2012).
[9] L. Gaudreau, A. Kam, G. Granger, S. A. Studenikin, P. Zawadzki, and A. S. Sachrajda, Appl. Phys. Lett. **95**, 193101 (2009).
[10] G. Granger, L. Gaudreau, A. Kam, M. Pioro-Ladrière, S. A. Studenikin, Z. R. Wasilewski, P. Zawadzki, and A. S. Sachrajda, Phys. Rev. B **82**, 075304 (2010).
[11] G. Granger *et al.*, Nat. Phys. **8**, 522 (2012).
[12] G. J. Schinner, H. P. Tranitz, W. Wegscheider, J. P. Kotthaus, and S. Ludwig, Phys. Rev. Lett. **102**, 186801 (2009).
[13] D. Harbusch, D. Taubert, H. P. Tranitz, W. Wegscheider, and S. Ludwig, Phys. Rev. Lett. **104**, 196801 (2010).
[14] See Supplemental Material at http://link.aps.org/supplemental/10.1103/PhysRevLett.118.067701 for a detailed discussion of the theoretical model, which includes Refs. [15–17].
[15] S. Ashhab, J. R. Johansson, A. M. Zagoskin, and F. Nori, Phys. Rev. A **75**, 063414 (2007).
[16] S. N. Shevchenko, S. Ashhab, and F. Nori, Phys. Rep. **492**, 1 (2010).
[17] *Landolt-Börnstein Numerical Data and Functional Relationships in Science and Technology*, edited by O. Madelung (Springer-Verlag, Berlin, 1987), Vol. 22.
[18] M. Field, C. G. Smith, M. Pepper, D. A. Ritchie, J. E. F. Frost, G. A. C. Jones, and D. G. Hasko, Phys. Rev. Lett. **70**, 1311 (1993).
[19] E. I. Rashba, Fiz. Tverd. Tela (Leningrad) **2**, 1224 (1960) [Sov. Phys. Solid State **2**, 1109 (1960)].
[20] G. Dresselhaus, Phys. Rev. **100**, 580 (1955).
[21] M. Florescu and P. Hawrylak, Phys. Rev. B **73**, 045304 (2006).
[22] U. Bockelmann and G. Bastard, Phys. Rev. B **42**, 8947 (1990).
[23] G. Granger, G. C. Aers, S. A. Studenikin, A. Kam, P. Zawadzki, Z. R. Wasilewski, and A. S. Sachrajda, Phys. Rev. B **91**, 115309 (2015).
[24] S. A. Studenikin and E. M. Skok, Phys. Status Solidi (b) **134**, 745 (1986).
[25] J. Danon and Y. V. Nazarov, Phys. Rev. B **80**, 041301(R) (2009).
[26] D. Kim *et al.*, Nature (London) **511**, 70 (2014).
[27] E. A. Laird, J. M. Taylor, D. P. DiVincenzo, C. M. Marcus, M. P. Hanson, and A. C. Gossard, Phys. Rev. B **82**, 075403 (2010).